frontiers in Physics

ORIGINAL RESEARCH
published: 31 August 2020
doi: 10.3389/fphy.2020.00282

Magnetic and Dielectric Properties of La and Ni Co-substituted $BiFeO_3$ Nanoceramics

Amit Srivastava[1], *Ashwani Kumar Singh*[2*], *O. N. Srivastava*[3], *H. S. Tewari*[4], *Khalid B. Masood*[5] *and Jai Singh*[4,5*]

[1] Department of Physics, TDPG College, VBS Purvanchal University, Jaunpur, India, [2] Center for Semiconductor and Nanotechnology Components (CCS Nano)—UNICAMP, Campinas, Brazil, [3] Department of Physics, Institute of Science, Banaras Hindu University, Varanasi, India, [4] Department of Pure and Applied Physics, Guru Ghasidas Vishwavidyalaya (A Central University), Bilaspur, India, [5] Department of Physics, Dr. Harisingh Gour University, Sagar, India

The increasing plead for the realization of ultra-fast, miniaturized, compact, and ultra-low power consumption in electronic as well as spintronic devices has propelled the quest for novel multiferroic materials that efficiently enable voltage control of magnetism. The present work reports the phase stability, magnetic and dielectric responses of polycrystalline $Bi_{1-x}La_xFe_{1-y}Ni_yO_3$ ($0 \leq x \geq 0.2$ and $0 \leq y \geq 0.2$) multiferroic ceramics synthesized through a simplistic sol–gel approach. The maneuver substitutions of La at A^- site of $BiFeO_3$ multiferroic eliminate the secondary phases formed owing to impurities. Rietveld refined XRD analysis reveals the structural transformation of the orthorhombic (Pbnm) phase as La substitution increases. However, an additional lattice distortion is induced as a result of the substitutions of Ni atoms at B^- site. A substantial enhancement in magnetic and dielectric responses has been found in the co-doped (Ni and La) sample at both A and B^- sites as a result of the size confinement of nano-crystallites, the exchange interaction between Fe^{3+} and Ni^{2+} ions, and corresponding variation in Fe–O–Fe bond angles. The dielectric constant has increased substantially in the low-frequency region with simultaneous substitutions of La and Ni at the sites of Bi and Fe, respectively. A careful observation of temperature-dependent magnetization curves (FC and ZFC) indicates a spin glass response with entangled ferromagnetic components. The experimental findings infer that the co-substitutions of La and Ni at their respective sites in $Bi_{1-x}La_xFe_{1-y}Ni_yO_3$ ($0 \leq x \geq 0.2$ and $0 \leq y \geq 0.2$) may significantly improve the ferromagnetic and dielectric responses of the studied nanoceramics.

Keywords: multiferroics, BFO, magnetization, dielectric constant and loss, nanoceramics

OPEN ACCESS

Edited by:
Aniruddha Dutta,
Queen's University, Canada

Reviewed by:
Chirag Garg,
IBM Research Almaden, United States
Monas Shahzad,
University of Central Florida, United States
Udai Bhanu,
Globalfoundries, United States

***Correspondence:**
Ashwani Kumar Singh
ashwanikumarsingh143@gmail.com
Jai Singh
jai.bhu@gmail.com

Specialty section:
This article was submitted to Condensed Matter Physics, a section of the journal Frontiers in Physics

Received: *23 June 2019*
Accepted: *23 June 2020*
Published: *31 August 2020*

Citation:
Srivastava A, Singh AK, Srivastava ON, Tewari HS, Masood KB and Singh J (2020) Magnetic and Dielectric Properties of La and Ni Co-substituted $BiFeO_3$ Nanoceramics. Front. Phys. 8:282. doi: 10.3389/fphy.2020.00282

INTRODUCTION

Multiferroics are among the special class of materials having ferroelectric and ferromagnetic phases simultaneously and being studied extensively in the recent past as they offer some of the most promising applications of technological importance [1–5]. Among various multiferroic materials, $BiFeO_3$ (BFO) has emerged as a potential material offering a wide range of viable applications in next-generation actuators, sensors, non-volatile memory devices (FeRAMs), and photovoltaics as it

has many intriguing properties such as robust ferroelectricity, magnetism, and photovoltaic effects [6–10]. Furthermore, BFO allows the tuning of magnetic properties by applying an electric field, i.e., EM coupling (converse ME coupling), and leads to controlled permeability with minimum power consumption. Energy harvesting applications of multiferroics through photovoltaic has been a pioneering area of study by its own and the combination of other ferroic properties leads it to a new track [11–14]. BFO shows multiferroic responses at room temperature, with Curie temperature (1,103 K) and Neel temperature (647 K) [15]. BFO crystal exhibits rhombohedral distorted perovskite structure with R3c space group ($a_r = 3.96$ Å and $\alpha_r = 0.6^\circ$) [16]. Nevertheless, pure and bulk BFO has shown poor performance in various technological applications because of low saturation magnetization, high current leakage, and poor magnetoelectric response at room temperature [17]. Therefore, there has been a continuous effort to improve the multiferroic properties of BFO through controlling their size (in the realm of nanoscale) and thus results in the origin of size-dependent magnetic and electric properties [18, 19]. On the other hand, the substitution of other atoms on either of A/B or A and B sites has proved to be another successful approach to alter the aforementioned properties. Despite tremendous advanced researches in the area of BFO, it is still difficult to develop a low-temperature synthesis protocol, which does not involve the formation of intermediate impurity phases [20, 21]. These impurity phases have a great influence on magnetic, electrical, and other properties of the multiferroic materials. At the same time, these impurity phases have also been responsible for the large leakage current discussed earlier, owing to the hopping of electrons, weak magnetoelectric coupling, and low resistivity. In recent demonstrations, it was found that chemical substitution or doping has been an effective way to remove the impurities and thus enhancing its multiferroic properties. Aliovalent and isovalent substitutions at Bi and Fe sites have been attempted to overcome this drawback and to enhance the magnetic, electric, and magnetoelectric properties [20–22]. Some earlier studies report that doping of isovalent elements at Bi^- sites eliminates or at least minimizes the formation of secondary phases [23]. It is also reported that it leads to a structural change as a result of imbalanced $6s^2$ lone pair and further affects the intrinsic properties like ferroelectric and magnetic responses. However, isovalent substitution at Fe^- site affects its magnetic properties without (or negligibly small) altering its ferroelectric behavior [24–28]. On the other hand, aliovalent doping at Bi or Fe site results to either fill or create oxygen vacancies [17, 29–32] and finally enhances the multiferroic properties of BFO. Doping of rare earth elements in BFO has been a subject of utmost importance as it leads to structural phase stability through the internal chemical pressure [33]. The small difference in atomic radii of rare earth dopant and Bi causes strong chemical pressure and thus affects the phase stability of the rhombohedral phase of doped BFO. In this context, La doping at Bi^- site has been of particular interest because of (1) the large difference in ionic radii of Bi^{3+} and La^{3+} and (2) the increase in dielectric constant and decrease in leakage current [34]. Similarly, the aliovalent doping of various divalent at the Fe^- site significantly improves the ferroelectric behavior of BFO [34]. Ni has been an effective candidate among various B^- site substituents in BFO with better multiferroic response [35–39].

Herein, keeping the aforementioned considerations, we have successfully synthesized La and Ni co-substituted BFO multiferroic ceramics, at A and B Fe site lattices, respectively, through a facile sol–gel approach. These substitutions lead to a structural transformation from rhombohedral to orthorhombic phase. The evolution of the new phase opens a new avenue of manipulating the ferromagnetic and ferroelectric properties of BFO. Therefore, a systematic study of the magnetic and ferroelectric properties of La and Ni co-substituted BFO vis-a-vis the structural modifications has been conducted.

MATERIALS AND METHODS

Chemicals

All the chemicals used in the present work were of analytical reagent grade and used as received without any further purification. Bismuth nitrate pentahydrate $Bi(NO_3)_3{\cdot}5H_2O$, iron nitrate nonahydrate $Fe(NO_3)_3{\cdot}9H_2O$, lanthanum nitrate hexahydrate $La(NO_3)_3{\cdot}6H_2O$, and nickel nitrate hexahydrate $Ni(NO_3)_2{\cdot}6H_2O$ were purchased from Sigma Aldrich whereas ethylene glycol and concentrated HNO_3 were procured from Fisher Scientific. Aqueous solutions used throughout the experiments were prepared by using ultrapure double-distilled water.

Synthesis

In a typical synthesis, a facile sol–gel method has been used to prepare $Bi_{1-x}La_xFe_{1-y}Ni_yO_3$ ($0 \leq x \geq 0.2$ and $0 \leq y \geq 0.2$) (BLFNO) powders. Briefly, stoichiometric amounts of the starting materials were dispersed in deionized water (100 ml), followed by a constant magnetic stirring at 200 rpm and 80°C. An additional quantity of bismuth nitrate (∼7.5 wt.%) was added to indemnify Bi owing to its volatile nature. A few drops of concentrated HNO_3 were also added to avoid the precipitation of bismuth hydroxide. Furthermore, ethylene glycol (50 ml) was added in the solution which forms an organic 3D tangled network and resulted in a transparent blackish-red solution. The as-obtained solution was further kept in an oven held at 150°C, and a xerogel powder was thus obtained. The xerogel powder was ground gently and calcined at 300°C for 4 h. The as-obtained powder was pelletized in the rectangular form through a hydraulic press at a pressure of 3.5 tons per square inch. The pellets were sintered at 550°C for 2.5 h and allowed to quench normally in the air.

Characterizations

The structural features and crystalline properties of the as-synthesized powder samples were accessed through a powder X-ray diffraction carried out by PANalytical X-ray diffractometer using CuK_α radiation ($\lambda = 1.5406$ Å at 40 kV and 30 mA), with scanning in the range 2θ of 15° to 80°. The as-obtained XRD data were further analyzed by Rietveld refinement using FullProf Programme. The microstructures and morphologies of the as-synthesized materials were studied by transmission

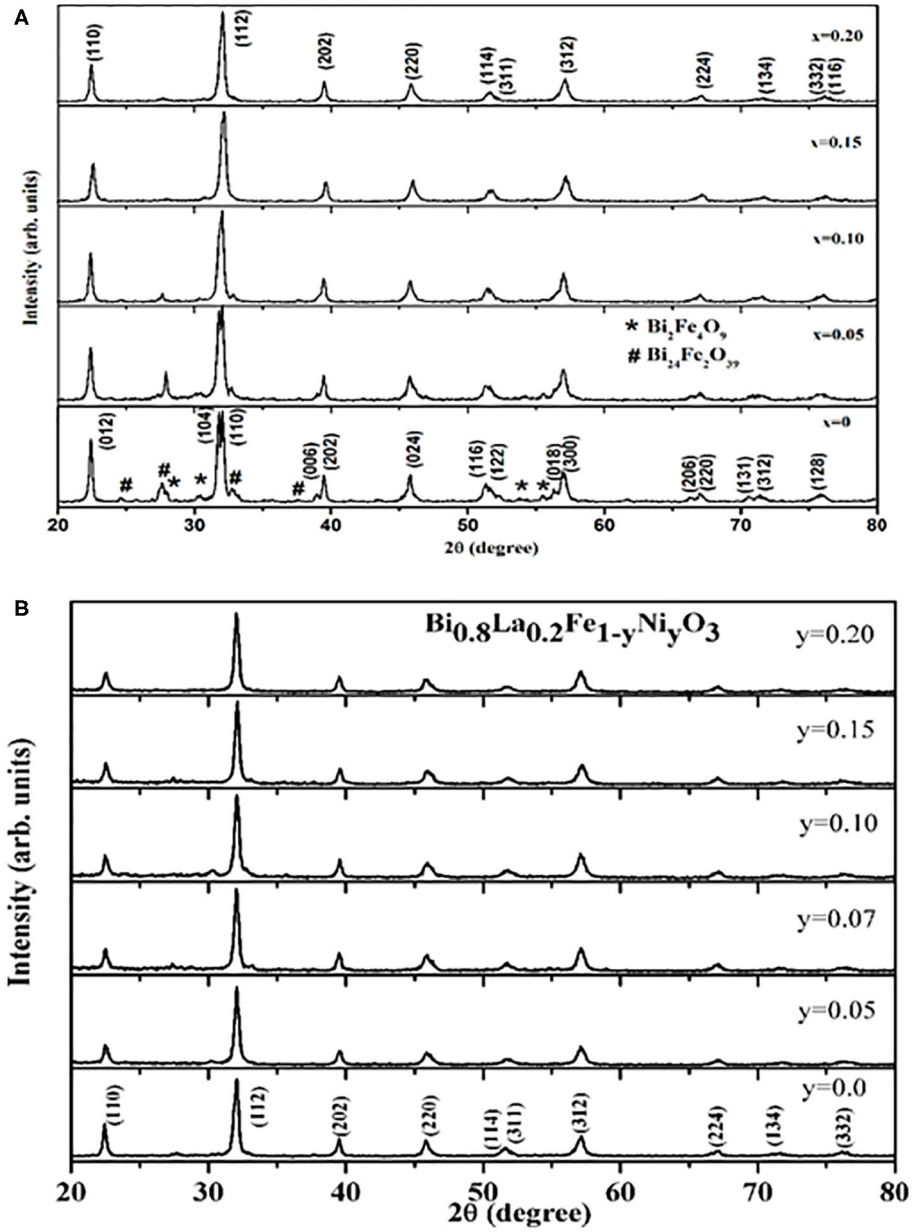

FIGURE 1 | (A) XRD patterns obtained for $Bi_{1-x}La_xFe_{1-y}Ni_yO_3$ ($x = 0.0, 0.05, 0.10, 0.15, 0.20$, and $y = 0.0$) samples at room temperature. **(B)** XRD patterns obtained for $Bi_{1-x}La_xFe_{1-y}Ni_yO_3$ ($x = 0.20$ and $y = 0.0, 0.05, 0.07, 0.1, 0.15, 0.20$) samples at room temperature.

electron microscope (TEM; TECNAI 20G^2, operated at an accelerating voltage of 200 kV) and scanning electron microscope (SEM-Quanta 200). Samples for TEM analysis were prepared by ultrasonically suspending the powder in double-distilled water and placing a drop of the suspension on a coated copper grid. Magnetization measurements of the as-synthesized samples were performed on a 7-T Quantum Design PPMS (VSM). The frequency dependence dielectric measurements were accessed through the HP4192A impedance analyzer at ambient conditions.

RESULTS AND DISCUSSION

Figure 1 describes X-ray diffraction patterns of all the as-synthesized materials $Bi_{1-x}La_xFe_{1-y}Ni_yO_3$ and reveals the polycrystalline behavior with good crystallinity of the samples. Diffraction peaks originated from (012), (104), (110), (006), (202), (024), (116), (112), (018), and (300) reflection planes have been the characteristic peaks of $BiFeO_3$ and indexed well with the known rhombohedral distorted perovskite structure having space group R3c (JCPDS No. 86-1518). The diffraction

pattern also exhibits some peaks owing to secondary phases, i.e., $Bi_2Fe_4O_9$ and $Bi_{24}Fe_4O_{39}$ [29, 40–42]. The formation of these impurity oxides and thereby substantial suppression with La doping at A site may be described by the fact that Bi^{3+} and Fe^{3+} ions have not been very stable in aqueous solution and get hydrolyzed in water rapidly. Oxide formation occurs fast

TABLE 1 | Refined structural parameters and tolerance factors of $Bi_{1-x}La_xFe_{1-y}Ni_yO_3$ nanoceramics.

$Bi_{1-x}La_xFe_{1-y}Ni_yO_3$	$x = 0.0$, $y = 0.0$	$x = 0.2$, $y = 0.0$ R3c phase	$x = 0.2$, $y = 0.0$ Pbnm phase	$x = 0.2$, $y = 0.05$	$x = 0.2$, $y = 0.07$	$x = 0.2$, $y = 0.10$	$x = 0.2$, $y = 0.15$	$x = 0.2$, $y = 0.2$
a (Å)	5.5815	5.5743	5.6000	5.6030	5.6040	5.6078	5.6102	5.6070
b (Å)	5.5815	5.5743	5.5898	5.5920	5.5930	5.6010	5.5986	5.5960
c (Å)	13.8740	13.7602	7.8421	7.8520	7.8540	7.8549	7.8560	7.8530
V ($Å^3$)	374.3089	370.2816	245.4803	246.0187	246.1692	246.7168	246.7511	246.4018
T	0.89089	0.88942	0.88942	088834	0.88791	0.88725	0.88617	0.88509
Fe–O(1)	2.19453	2.10184	2.0213	2.0228 (5)	2.0387 (7)	2.0479 (7)	2.0056 (7)	1.9723 (5)
Fe–O(2)	1.89068	1.94454	1.971 (8)	1.5151 (8)	1.5335 (9)	1.5673 (10)	1.5335 (6)	1.4940 (7)
Fe–O(2)	–	–	2.4798 (13)	2.4892 (13)	2.4939 (16)	2.6588 (20)	2.6559 (10)	2.6641 (13)
Fe–O–Fe	152.1987	155.1669	156.14 (13)	157.01 (13)	157.43 (14)	157.46 (20)	156.16 (9)	155.62 (13)
χ^2	2.54	1.83	1.91	1.499	1.846	2.099	1.709	1.566

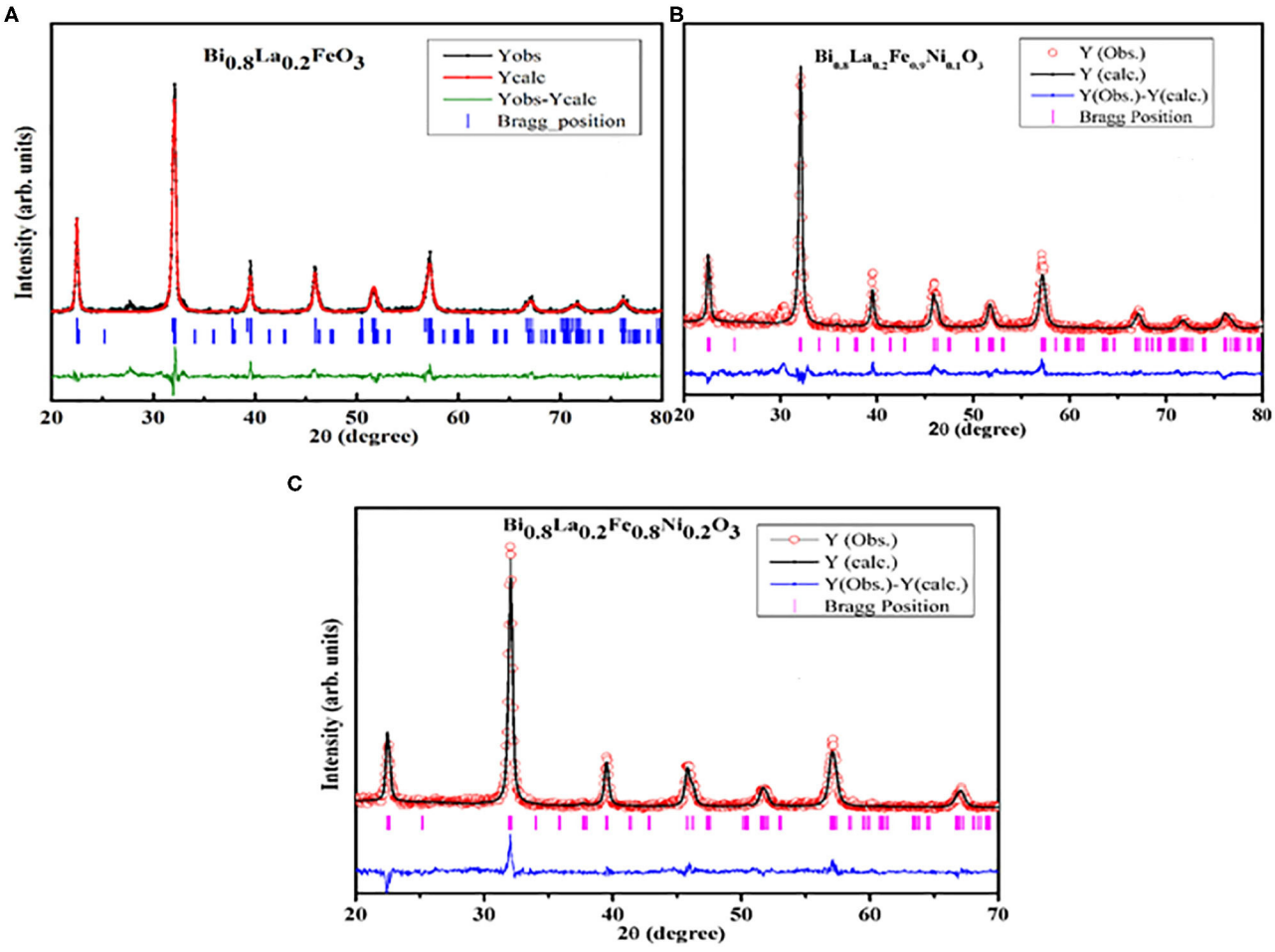

FIGURE 2 | Observed, calculated, and difference Rietveld refined XRD patterns of $Bi_{1-x}La_xFe_{1-y}Ni_yO_3$ samples: **(A)** $x = 0.20$ and $y = 0.0$, **(B)** $x = 0.20$ and $y = 0.10$, **(C)** $x = 0.20$ and $y = 0.20$.

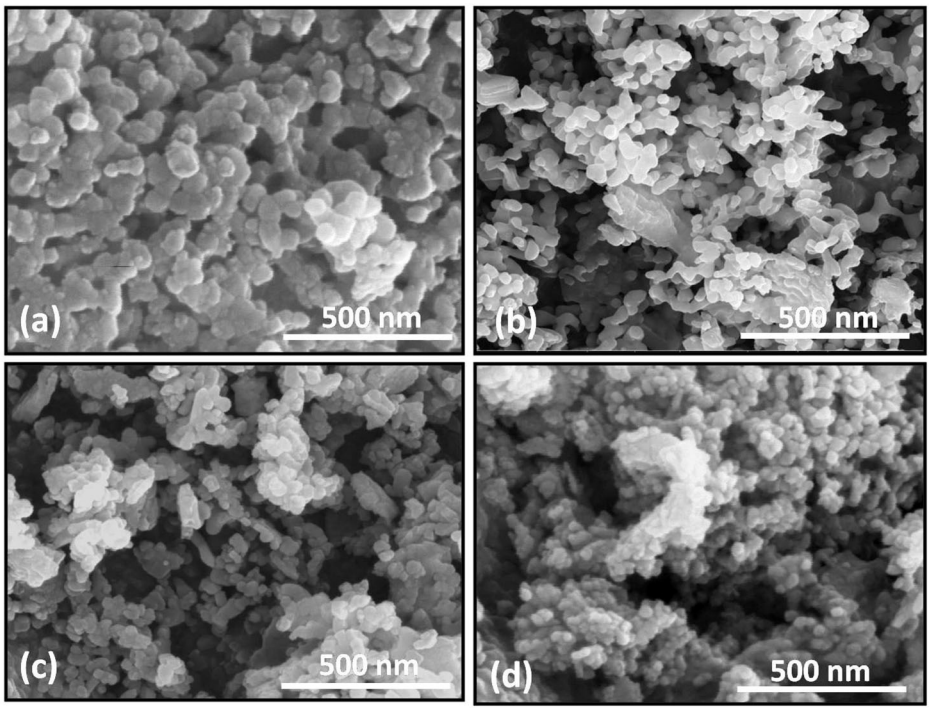

FIGURE 3 | SEM images of $Bi_{1-x}La_xFe_{1-y}Ni_yO_3$: **(a)** $x = 0$, $y = 0$; **(b)** $x = 0.20$, $y = 0$; **(c)** $x = 0.2$, $y = 0.05$; **(d)** $x = 0.2$, $y = 0.2$.

from the respective hydrolyzed contents in a binary solution of water–ethylene glycol. Because ethylene glycol molecule contains two hydroxyl groups and forms a 3D network, the oxide formation reaction gets increased in water–ethylene glycol solution. Oxide formation usually occurs following the reaction, in the present case:

$$27Bi(OH)_3 + 7Fe(OH)_3 \longrightarrow BiFeO_3 + Bi_{24}Fe_2O_{39} + Bi_2Fe_4O_9 + 51\ H_2O$$

The incorporation of La significantly reduces the probability of formation of hydroxides and volatilization of Bi leading to the oxygen ion vacancies in the lattice, in turn restricting the formation of the undesired oxides.

The XRD patterns of the studied $Bi_{1-x}La_xFe_{1-y}Ni_yO_3$ samples also reveal that the peak splitting behavior decreases gradually with increasing x contents. Furthermore, the diffraction peaks (104), (110) and (006), (202) get merged to the respective single peaks, suggesting the distortion of the rhombohedral structure by La substitutions [40]. It is known that with the decrease in the average A^- site ionic radius, rhombohedral to orthorhombic phase transition occurs in $BiFeO_3$ system because of the chemical pressure exerted by a relatively small rare earth (RE) substitution at Bi site [40]. Moreover, the co-substitutions of La and Ni at their respective sites lead to a continuous shift in 2θ values toward a higher angle as a result of a significant decrease in the unit cell parameters and the volume as evident from **Table 1** also. **Figure 2** depicts the Rietveld refined XRD patterns of the selective samples. The pseudo-Voigt function was used to fit the peak profile of pure BFO (space group R3c) and for La and Ni co-substituted samples (space group Pbnm) [40]. The observed, calculated, and difference for XRD patterns of $Bi_{1-x}La_xFe_{1-y}Ni_yO_3$ have been found in fairly well-agreement. The tolerance factor τ ($\tau = (r_A + r_O)/\sqrt{2}(r_B + r_O)$, where r_A, r_B, and r_O represent the ionic radii of the A, B, and O sites, respectively) has been calculated and summarized in **Table 1**. Ni substitution leads to a decrease in tolerance factor and thereby the driving force for octahedral rotation increases.

The insight of the morphological aspects of $Bi_{1-x}La_xFe_{1-y}Ni_yO_3$ ($x = 0.0$, 0.2 with $y = 0.0$ and 0.2) nanoceramic samples has been studied by employing scanning electron microscopy. **Figure 3** represents the typical SEM micrograph of as-synthesized samples. It depicts the agglomeration of nanosized particles and, in turn, reveals that the progressive doping of La and Ni contents affects the morphologies of the sample. SEM micrograph of pristine BFO indicates that the grains have been rather non-uniform and the grain size varies in the range ∼100–150 nm. Moreover, the SEM micrographs of La and Ni co-substituted $BiFeO_3$ point that the particle morphology slightly changes with reduced grain size. It infers the effect on the crystallization habit of BFO particles by doping contents.

TEM studies have been carried out to further investigate the morphological aspects of $Bi_{1-x}La_xFe_{1-y}Ni_yO_3$ ($x = 0.0$, 0.2 with $y = 0.0$ and 0.2) nanoceramics and displayed in **Figure 4**. The average particle size of the sample decreases from 100–150 nm with $x = 0.1$; $y = 0.0$ to 50–60 nm with $x = 0.2$; $y = 0.2$ which results because of the unit cell volume decrease. The inset shows

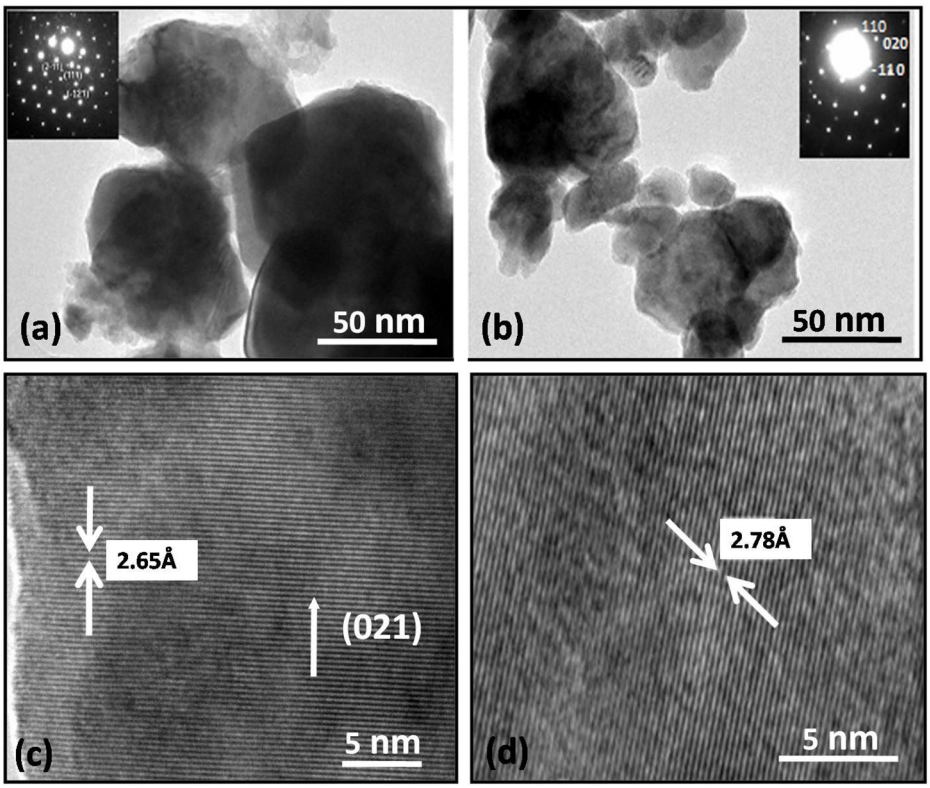

FIGURE 4 | TEM images of $Bi_{1-x}La_xFe_{1-y}Ni_yO_3$: **(a)** $x = 0.0$, $y = 0$; **(b)** $x = 0.20$, $y = 0$. Inset in **(a,d)** shows SAED pattern for rhombohedral **(c,d)** HRTEM images of $Bi_{1-x}La_xFe_{1-y}Ni_yO_3$ ($y = 0.0$ and 0.10 with $x = 0.20$, for both).

the selected area electron diffraction (SAED) patterns of pristine BFO and Ni-doped BFO samples. It reveals the hexagonal pattern (inset of **Figure 4a**) indexed with rhombohedral structure whereas the diffraction pattern (inset of **Figure 4b**) of Ni-doped BFO possesses the orthorhombic symmetry (Pbnm).

The temperature and field dependence magnetization of the as-synthesized samples have been investigated for assessing the magnetic behavior of the nanoceramics. **Figures 5A,B** traces the room temperature magnetization hysteresis (M-H) loop of the samples. The magnetization increases linearly with an increasing magnetic field, suggesting the existence of weak ferromagnetism arising as a result of canting of antiferromagnetic sublattices, for pristine BFO. The magnetic moment gets enhanced substantially with La doping at A^- site in $BiFeO_3$. Such enhancement has already been reported elsewhere [41, 42]. **Figures 5A,B** indicates that magnetization changes with Ni^- doping in $Bi_{1-x}La_xFe_{1-y}Ni_yO_3$ ($x = 0.2$ and $y = 0.05$, 0.07, 0.10, 0.15, and 0.20) even in the low field range, i.e., up to 1 T. It can also be observed that the magnetization increases to a maximum for $y = 0.10$ and further decreases with a higher content of Ni. It is reported that the magnetization has been induced in $BiFeO_3$ by regulating the particle size smaller to the enduring spin periodicity of 62 nm as well as by chemical substitution [29, 40, 43]. In the present study, the particle sizes have been found close to the spin periodicity so the reduction in particle size plays a vital role in the enhanced magnetization. The enhancement in the magnetization of $Bi_{1-x}La_xFe_{1-y}Ni_yO_3$ can also be attributed to the substitution of a small amount of Ni^{2+} doping at B^- site which perturbs the Fe–O–Fe bond angles (**Table 1**). As the superexchange interaction has been sensitive to bond angles, the spiral structure may get destroyed completely by co-substitution of La^{3+} and Ni^{2+}, and thereby leads to the enhancement in magnetization [39].

The ZFC and FC curves of $Bi_{1-x}La_xFe_{1-y}Ni_yO_3$ ($x = 0.2$ and $y = 0.0$, 0.05, 0.07, 0.10, 0.15, and 0.20) nanoceramics under applied magnetic field of 500 Oe reveal a non-monotonic temperature dependence and irreversibility. It also shows a distinct separation of up to 300 K between FC and ZFC curves for pristine BFO owing to the relaxation process [44]. **Figure 5C** shows that the separation increases with lowering the temperature, indicating the existence of some glass-like component, and has been consistent with the assumption that the magnetic properties of BFO ceramic get readily affected by the nanostructured nature [45].

The dielectric constant and dielectric loss of the as-synthesized $Bi_{1-x}La_xFe_{1-y}Ni_yO_3$ nanoceramics have been investigated in the frequency range 100 Hz to 1 MHz at room temperature, for evaluating the dielectric performance. The dielectric properties of the samples in this frequency range are rarely available because of the persistence of leakage current. **Figure 6A** demonstrates

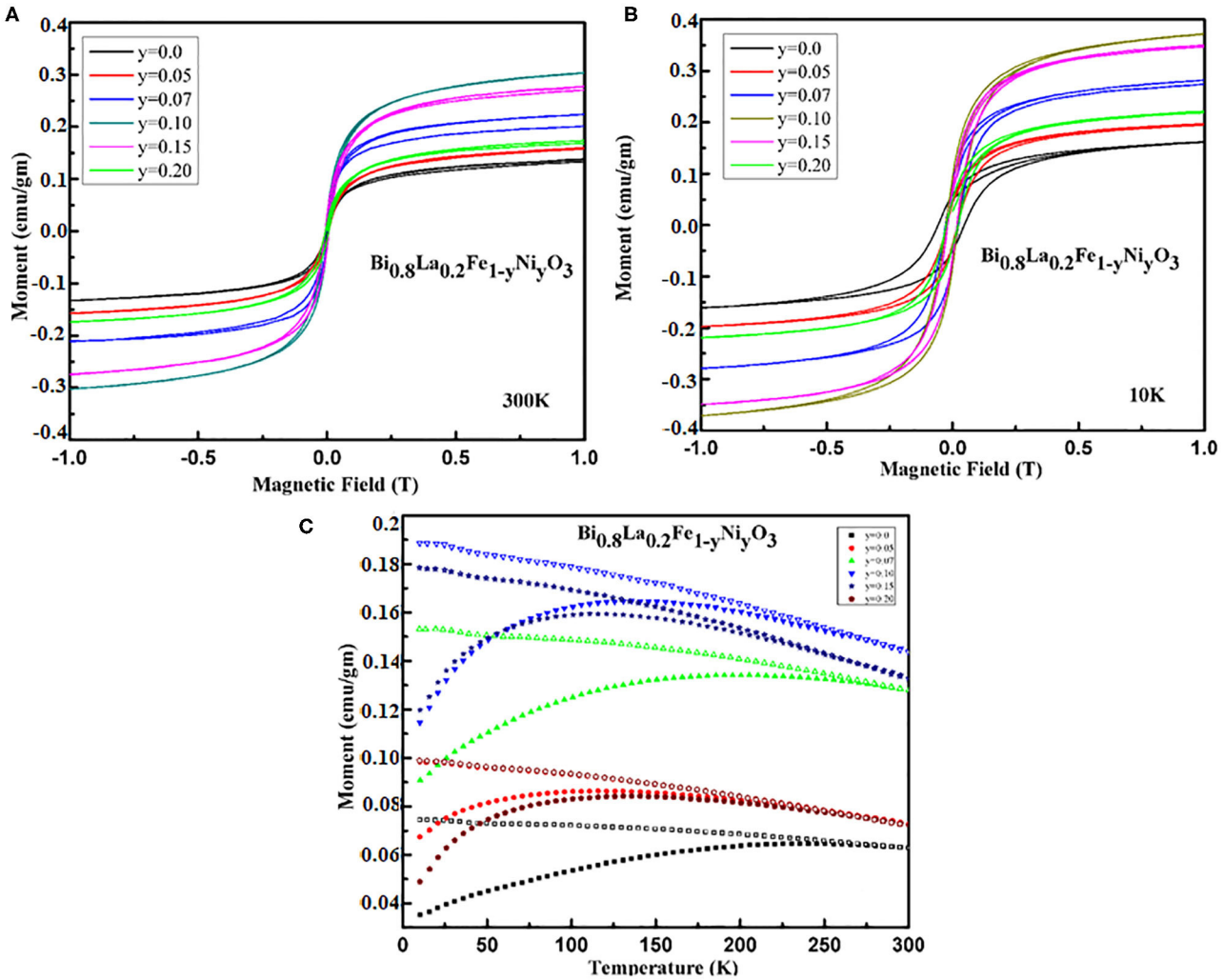

FIGURE 5 | Field dependences of the magnetization obtained for $Bi_{1-x}La_xFe_{1-y}Ni_yO_3$ samples **(A)** $x = 0.20$ with $y = 0.0, 0.05, 0.07, 0.1, 0.15, 0.20$ at room temperature and **(B)** $x = 0.20$ with $y = 0.0, 0.05, 0.1, 0.15, 0.20$ at 10 K. **(C)** Temperature dependence magnetization obtained $Bi_{1-x}La_xFe_{1-y}Ni_yO_3$ ($x = 0.20$ and $y = 0.0, 0.05, 0.07, 0.1, 0.15, 0.20$) samples at constant field 500 Oe.

the decrease in the values of dielectric constant with increasing frequency. This variation of dielectric constant points out the dispersion that occurred led by Maxwell interfacial polarization and has been in accord with the Koops phenomenological theory [46]. The dispersion of dielectric constant may be caused by the hopping of electrons between Fe^{2+} and Fe^{3+} ions. The large values of the dielectric constant in $Bi_{1-x}La_xFe_{1-y}Ni_yO_3$ can be understood as the replacement of Fe^{3+} by Ni^{2+} that has been expected to introduce a higher density of vacancies and increase the probability of hopping conduction mechanism. The initial slow decrease in the dielectric constant has been consistent with the Koops model [46]. Moreover, the polycrystalline samples have high grain boundary density and so the nature of the grains and grain boundaries affects the electrical properties [47]. The inhomogeneity occurred because of grains and grain boundaries that lead to high dielectric value.

The room temperature frequency dependence of dielectric loss for $Bi_{1-x}La_xFe_{1-y}Ni_yO_3$ nanoceramics is presented in **Figure 6B**. It shows that the dielectric loss decreases smoothly with the increase in the frequency. The dielectric loss increases for all the samples with decreasing frequency without having any loss peak. It signifies that the synthesized material is homogeneous and stoichiometric with uniform distribution of the grain/particles.

CONCLUSION

Summarily, $Bi_{1-x}La_xFe_{1-y}Ni_yO_3$ nanoceramics have successfully been synthesized by ethylene glycol–based sol–gel method. The XRD pattern of the pristine $BiFeO_3$ reveals the rhombohedral distorted perovskite structure having space group R3c and substantial decrement in impurity phases has also been

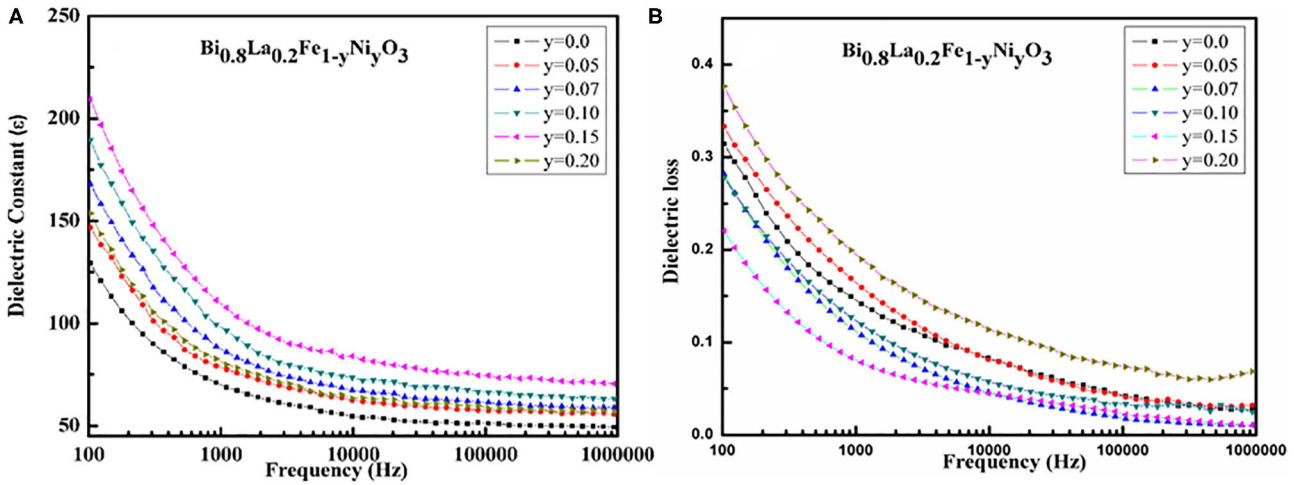

FIGURE 6 | (A) Variation of dielectric constant with frequency for $Bi_{1-x}La_xFe_{1-y}Ni_yO_3$ ($x = 0.20$ with $y = 0.0, 0.05, 0.07, 0.1, 0.15, 0.20$) ceramics. **(B)** Variation of dielectric loss, with frequency for $Bi_{1-x}La_xFe_{1-y}Ni_yO_3$ ($x = 0.20$ with $y = 0.0, 0.05, 0.07, 0.1, 0.15, 0.20$) ceramics.

observed with La substitution at A^- site in $BiFeO_3$. Rietveld refinement suggests the induced lattice distortion with La and Ni co-substitution in $Bi_{1-x}La_xFeO_3$ nanoceramics. Enhancement in the magnetic behavior has been observed with Ni contents in the sample as a result of the suppression of cycloidal spin structure arising from the size confinement effect, exchange interaction between Fe^{3+} and Ni^{2+} ions, and distortion in Fe–O–Fe bond angle. Notable enhancement in dielectric ordering and reduction in loss tangent have also been observed in the samples by the co-substitution of La and Ni in $BiFeO_3$ nanoceramics.

DATA AVAILABILITY STATEMENT

The datasets generated for this study are available on request to the corresponding author.

AUTHOR CONTRIBUTIONS

ASr performed the sample preparation, collected the experimental data, and completed the writing of the manuscript. ASi collected the structural data like XRD and analyzed it. OS, KM, and JS helped in the manuscript writing. HT was involved in data analysis and editing the draft. All authors contributed to the article and approved the submitted version.

ACKNOWLEDGMENTS

The authors are thankful to Dr. A. Banerjee (IUC–Indore) for his help with magnetic measurements and data analysis. ASr gratefully acknowledges the financial support from the University Grants Commission (UGC)–India, under Raman Fellowship with File No. F 5-139/2016 (IC).

REFERENCES

1. Rojac T, Bencan A, Drazic G, Sakamoto N, Ursic H, Jancar B, et al. Domain-wall conduction in ferroelectric $BiFeO_3$ controlled by the accumulation of charged defects. *Nat Mater.* (2017) **16**:322–7. doi: 10.1038/nmat4799
2. Yin RQ, Dai BW, Zheng P, Zhou JJ, Bai WF, Wen F, et al. Pure-phase $BiFeO_3$ ceramics with enhanced electrical properties prepared by two-step sintering. *Ceram Int.* (2017) **43**:6467–71. doi: 10.1016/j.ceramint.2017.02.063
3. Hill NA. Why are there so few magnetic ferroelectrics? *J Phys Chem B.* (2000) **104**:6694–709. doi: 10.1021/jp000114x
4. Wang J, Neaton JB, Zheng H, Nagarajan V, Ogale SB, Liu B, et al. Epitaxial $BiFeO_3$ multiferroic thin film heterostructures. *Science.* (2003) **299**:1719–22. doi: 10.1126/science.1080615
5. Spaldin NA, Ramesh R. Advances in magnetoelectric multiferroics. *Nat Mater.* (2019) **18**:203–12. doi: 10.1038/s41563-018-0275-2
6. Wu J, Zhen F, Xiao D, Zhu J, Wang J. Multiferroic bismuth ferrite-based materials for multifunctional applications: ceramic bulks, thin films, and nanostructures. *Prog Mater Sci.* **84**:335–402. doi: 10.1016/j.pmatsci.2016.09.001
7. Rhaman MM, Matin MA, Hossain MN, Mozahid FA, Hakim MA, Rizvi MH, et al. Bandgap tuning of Sm and Co co-doped BFO nanoparticles for photovoltaic application. *J Electronic Mater.* (2018) **47**:6954–8. doi: 10.1007/s11664-018-6597-7
8. Waghmare SD, Jadhav VV, Shaikh SF, Mane RS, Rhee JH, O'Dwyer C. Sprayed tungsten-doped and undoped bismuth ferrite nanostructured films for reducing and oxidizing gas sensor applications. *Sensors Actuators A.* (2018) **271**:37–43. doi: 10.1016/j.sna.2018.01.008
9. Eerenstein W, Mathur ND, Scott JF. Multiferroic and magnetoelectric materials. *Nature.* (2006) **442**:759–65. doi: 10.1038/nature05023
10. Catalan G, Scott JF. Physics and applications of Bismuth Ferrite. *Adv Mater.* (2009) **21**:2463–85. doi: 10.1002/adma.200802849
11. Belinicher VI, Sturman BI. The photogalvanic effect in media lacking a center of symmetry. *Sov Phys Usp.* (1980) **23**:199–209. doi: 10.1070/PU1980v023n03ABEH004703
12. Ji W, Yao K, Liang YC. Bulk photovoltaic effect at visible wavelength in epitaxial ferroelectric $BiFeO_3$ thin films. *Adv Mater.* (2010) **22**:1763-6. doi: 10.1002/adma.200902985

13. Ji W, Yao K, Liang YC. Evidence of bulk photovoltaic effect and large tensor coefficient in ferroelectric $BiFeO_3$ thin films. *Phys Rev B.* (2011) **84**:094115. doi: 10.1103/PhysRevB.84.094115
14. Yang SY, Martin LW, Byrnes SJ, Conry TE, Basu SR, Paran D, et al. Photovoltaic effects in $BiFeO_3$. *Appl Phys Lett.* (2009) **95**:062909. doi: 10.1063/1.3204695
15. Verma KC, Kotnala RK. Tailoring the multiferroic behavior in $BiFeO_3$ nanostructures by Pb doping. *RSC Adv.* (2016) **6**:57727–38. doi: 10.1039/C6RA12949H
16. Kubel F, Schmid H. Structure of a ferroelectric and ferroelastic monodomain crystal of the perovskite $BiFeO_3$. *Acta Crystallogr B Struct Sci. B.* (1990) **46**:698–702. doi: 10.1107/S0108768190006887
17. Dutta DP, Jayakumar OD, Tyagi AK, Girija KG, Pillai CGS, Sharma G. Effect of doping on the morphology and multiferroic properties of $BiFeO_3$ nanorods. *Nanoscale.* (2010) **2**:1149–54. doi: 10.1039/c0nr00100g
18. Zhang XY, Lai CW, Zhao X, Wang DY, Dai JY. Synthesis and ferroelectric properties of multiferroic $BiFeO_3$ nanotube arrays. *Appl Phys Lett.* (2005) **87**:143102. doi: 10.1063/1.2076437
19. Gao F, Yuan Y, Wang KF, Chen XY, Chen F, Liu JM, et al. Preparation and photoabsorption characterization of $BiFeO_3$ nanowires. *Appl Phys Lett.* (2006) **89**:102506. doi: 10.1063/1.2345825
20. Kothari D, Reddy VR, Gupta A, Phase DM, Lakshmi N, Deshpande SK, et al. Study of the effect of Mn doping on the $BiFeO_3$ system. *J Phys Condens Matter.* (2007) **19**:136202. doi: 10.1088/0953-8984/19/13/136202
21. Kumar M, Yadav KL. Study of room temperature magnetoelectric coupling in Ti substituted bismuth ferrite system. *J Appl Phys.* (2006) **100**:074111. doi: 10.1063/1.2349491
22. Chung C-F, Lin JP, Wu JM. Influence of Mn and Nb dopants on electric properties of chemical-solution-deposited $BiFeO_3$ films. *Appl Phys Lett.* (2006) **88**:242909. doi: 10.1063/1.2214138
23. Jangid S, Barbar S, Bala I, Roy M. Structural, thermal, electrical and magnetic properties of pure and 50% La doped $BiFeO_3$ ceramics. *Phys B Condens Matter.* (2012) **407**:3694–9. doi: 10.1016/j.physb.2012.05.013
24. Khomchenko VA, Karpinsky DV, Paixão JA. Magnetostructural correlations in $BiFeO_3$-based multiferroics. *J Mater Chem C.* (2017) **5**:3623–9. doi: 10.1039/C7TC00833C
25. Koval V, Skorvanek I, Reece M, Mitoseriu L, Yan H. Effect of dysprosium substitution on crystal structure physical properties of multiferroic $BiFeO_3$ ceramics. *J Eur Ceram Soc.* (2014) **34**:641–51. doi: 10.1016/j.jeurceramsoc.2013.10.002
26. Bielecki J, Svedlindh P, Tibebu DT, Cai S, Eriksson S-G, Borjesson L, et al. Structural and magnetic properties of isovalently substituted multiferroic $BiFeO_3$: insights from Raman spectroscopy. *Phys Rev B Condens Matter Phys.* (2012) **86**:184422. doi: 10.1103/PhysRevB.86.184422
27. Dutta DP, Mandal BP, Naik R, Lawes G, Tyagi AK. Magnetic, ferroelectric, magnetocapacitive properties of sonochemically synthesized Sc-doped $BiFeO_3$ nanoparticles. *J Phys Chem C.* (2013) **117**:2382–9. doi: 10.1021/jp310710p
28. Belik AA, Abakumov AM, Tsirlin AA, Hadermann J, Kim J, Tendeloo GV, et al. Structure and magnetic properties of $BiFe_{0.75}Mn_{0.25}O_3$ perovskite prepared at ambient and high pressure. *Chem Mater.* (2011) **23**:4505–14. doi: 10.1021/cm201774y
29. Zhao J, Zhang X, Liu S, Zhang W, Liu Z. Effect of Ni substitution on crystal structure magnetic properties of $BiFeO_3$. *J Alloys Compd.* (2013) **557**:120–3. doi: 10.1016/j.jallcom.2013.01.005
30. Guo R, Fang L, Dong W, Zheng F, Shen M. Enhanced photocatalytic activity ferromagnetism in Gd doped $BiFeO_3$ nanoparticles. *J Phys Chem C.* (2010) **114**:21390–6. doi: 10.1021/jp104660a
31. Lotey GS, Verma NK. Structural magnetic electrical properties of Gd-doped $BiFeO_3$ nanoparticles with reduced particle size. *J Nanopart Res.* (2012) **14**:742–7. doi: 10.1007/s11051-012-0742-7
32. Singh H, Yadav KL. Dielectric magnetic magnetoelectric properties of La Nb codoped bismuth ferrite. *J Phys Condens Matter.* (2011) **23**:385901. doi: 10.1088/0953-8984/23/38/385901
33. Yu B, Li M, Liu J, Guo D, Pei L, Zhao X. Effects of ion doping at different sites on electrical properties of multiferroic $BiFeO_3$ ceramics. *J Phys D Appl Phys.* (2008) **41**:065003. doi: 10.1088/0022-3727/41/6/065003
34. Das R, Sarkar T, Mandal K. Multiferroic properties of Ba^{2+} Gd^{3+} co-doped bismuth ferrite: magnetic, ferroelectric impedance spectroscopic analysis. *J Phys D Appl Phys.* (2012) **45**:455002. doi: 10.1088/0022-3727/45/45/455002
35. Mishra DK, Qi X. Energy levels photoluminescence properties of nickel-doped bismuth ferrite. *J Alloys Compd.* (2010) **504**:27–31. doi: 10.1016/j.jallcom.2010.05.107
36. Xu X, Liu W, Zhang H, Guo M, Wu P, Wang S, et al. The abnormal electrical optical properties in Na Ni codoped $BiFeO_3$ nanoparticles. *J Appl Phys.* (2015) **117**:174106–8. doi: 10.1063/1.4919822
37. Lee SM, Cho A, Cho YS. Enhanced optical and piezoelectric characteristics of transparent Ni-doped $BiFeO_3$ thin films on a glass substrate. *RSC Adv.* (2016) **6**:16602–7. doi: 10.1039/C5RA27674H
38. Singh SK, Maruyama K, Ishiwara H. Reduced leakage current in La and Ni codoped $BiFeO_3$ thin films. *Appl Phys Lett.* (2007) **91**:112913–15. doi: 10.1063/1.2784968
39. Sharma J, Hamid B, Kumar A, Srivastava AK. Investigation of structural and dielectric properties of La-Ni doped bismuth nanoferrite. *J Mater Sci Mater Electron.* (2017) **29**:1107–17. doi: 10.1007/s10854-017-8012-1
40. Srivastava A, Singh HK, Awana VPS, Srivastava ON. Enhancement in magnetic dielectric properties of La Pr co substituted $BiFeO_3$. *J Alloys Compd.* (2013) **552**:336–44. doi: 10.1016/j.jallcom.2012.09.142
41. Uniyal P, Yadav KL. Pr doped bismuth ferrite ceramics with enhanced multiferroic properties. *J Phys Condens Matter.* (2009) **21**:405901–6. doi: 10.1088/0953-8984/21/40/405901
42. Wang DY, Chan NY, Zheng RK, Kong C, Lin DM, Dai JY, et al. Multiferroism in orientational engineered (La, Mn) co-substituted BiFeO3 thin films. *J Appl Phys.* (2011) **109**:114105–6. doi: 10.1063/1.3594745
43. Lin Y-H, Jiang Q, Wang Y, Nan C-W, Chen L, Yu J. Enhancement of ferromagnetic properties in $BiFeO_3$ polycrystalline ceramic by La doping. *Appl Phys Lett.* (2007) **90**:172507–3. doi: 10.1063/1.2732182
44. Mao J, Sui Y, Zhang X, Wang X, Su Y, Wang Y, et al. Evidence of two distinct dynamical freezing processes in single-layered perovskite $La_{0.7}Sr_{0.3}CoO_4$. *J Phys Condens Matter.* (2011) **23**:336001–7. doi: 10.1088/0953-8984/23/33/336001
45. Park TJ, Papaefthymiou GC, Viescas AJ, Moodenbaugh AR, Wong SS. Size-dependent magnetic properties of single-crystalline multiferroic $BiFeO_3$ nanoparticles. *Nano Lett.* (2007) **7**:766–72. doi: 10.1021/nl063039w
46. Koops CG. On the dispersion of resistivity and dielectric constant of some semiconductors at audiofrequencies. *Phys Rev.* (1951) **83**:121–5. doi: 10.1103/PhysRev.83.121
47. Larson AM, Moetakef P, Gaskell K, Brown CM, King G, Rodriguez EE. Inducing ferrimagnetism in insulating hollandite $Ba_{1.2}Mn_8O_{16}$. *Chem Mater.* (2015) **27**:515–25. doi: 10.1021/cm503801j

Conflict of Interest: The authors declare that the research was conducted in the absence of any commercial or financial relationships that could be construed as a potential conflict of interest.